

Ambient temperature effect on single-bubble sonoluminescence in different concentrations of sulfuric acid solutions

Kh. Imani, F. Bemani, M. Silatani, and R. Sadighi-Bonabi*

¹*Department of Physics, Sharif University of Technology, 11365-91 Tehran, Iran*

(Received 11 July 2011; revised manuscript received 22 November 2011; published 31 January 2012)

The effect of ambient temperature on the parameters of the single-bubble sonoluminescence in sulfuric acid (SA) diluted in water is studied. Using a hydrochemical model, three dominant instabilities of shape, Bjerknes, and diffusion are considered. The phase diagrams of the bubble in the $(R_0 - P_a)$ space are presented, and the parametric dependence of the light intensity is discussed. In contrast to water, the calculated thermal-bremsstrahlung mechanism of light emission at the fixed degassing condition of high SA concentrations shows that, with increasing the temperature of aqueous SA solutions, the light intensity increases. However, at diluted SA solutions similar to water, the light intensity decreases with increasing the ambient temperature. For 50 wt % SA, it was observed that the emitted light was almost temperature independent. Furthermore, it is found that, at the fixed temperatures of 20 °C, 10 °C, and 0 °C, the aqueous solutions of 65 wt %, 50 wt %, and 45 wt % SA, respectively, have the maximum light emission.

DOI: [10.1103/PhysRevE.85.016329](https://doi.org/10.1103/PhysRevE.85.016329)

PACS number(s): 78.60.Mq

I. INTRODUCTION

Since the stable demonstration of sonoluminescence (SL) by Gaitan *et al.*, various aspects of this unique phenomenon have been studied intensively [1,2]. In addition, valuable reports about single-bubble SL (SBSL), multibubble SL (MBSL) also were studied extensively [2]. However, due to the bubble high stability and longer glowing time, the research on SBSL is pursued more. Temperatures and pressures are much higher in SBSL than in MBSL. This is because of the isolation of the SB from perturbations.

The recent paper on SL using sulfuric acid (SA) denotes that the response of the gas bubbles in this host liquid are very different from what has been reported for water in several aspects [3–7]. Several observations of SBSL in SA are reported in the interesting dynamical states of the SL bubble, such as moving SBSL (MSBSL) [3,8,9], jittering SBSL, and regular lattices of luminescing bubbles [3]. This is due to various features of SA, such as low vapor pressure (3 orders of magnitude less than that of water), a high solubility of sonolysis products, producing various SAs aqueous with different viscosities and transparency for the wavelengths down to 200 nm. Extremely intense SL in SA aqueous solutions has been discovered in both SBSL and MBSL on the order of 2700 times brighter than SL in water, which shows the difference between SBSL in SA and water [6]. SBSL can be produced in water by an acoustic pressure ranging from 1.3 to 1.5 bar. Using SA solutions as the host liquids, Ar bubbles can be driven at higher acoustic pressures than that of water [3].

It is reported that the emitted light intensity of SBSL is very sensitive to parameters, such as ambient pressure [10–12], ambient temperature [10,13–16], noble gas content [2], and host liquid concentration [3,17]. One of the interesting observations in experiments of SBSL is the high dependency of light emission on ambient temperature. Those experimental papers verify that SL in cold water emits a

much higher intensity of light where the radiation intensity at 0 °C is 2 orders of magnitude higher than that of water at 40 °C.

Although valuable experimental papers as well as theoretical papers have reported on the ambient temperature effect of SBSL in water, it is not extended to the other liquids, such as SA solutions [10,13–16]. Recently, a numerical paper on the SBSL of the Ar bubble in some concentrations of SA solutions was reported, which was limited to only one value of ambient temperature at 20 °C [17]. More recently, the behavior of SBSL in water and one concentration of SA also were reported [18]. However, due to the lack of data and results in different concentrations of SA, a comprehensive consequence was not deduced. The hereby research provides a more detailed investigation of the ambient temperature effect on the physical parameters of the host liquid and SBSL intensity. This paper extends the behavior of SBSL in different concentrations of SA at various ambient temperatures, which is much more compatible to the available experimental results, and the physics reason behind this behavior also is explained.

In this paper, based on the hydrochemical model, which will be discussed later in the paper, the numerical study of SBSL in SA solutions, the effect of the ambient temperature on the SL intensity of various concentrations of SA and its relation to the liquid physical parameters, is discussed. It was very interesting to see that, in contrast to the earlier reports of SBSL for water [10,15,16], at the higher SA concentrations, by decreasing the SA aqueous solution temperature, the light intensity decreases. In the present paper, for the SA solutions containing the Ar gas, the maximum SL radiation is achieved for the solution with a SA concentration of around 50 wt % at 10 °C. It is noticed that a further decrease in the ambient temperature down to 0 °C results in the maximum SL radiation in a 45 wt % SA concentration. Furthermore, we notice that the light intensity of 50 wt % SA aqueous solution is almost temperatures independent. For this concentration, the irradiance at 10 °C is the maximum. These calculations and achievements are discussed in detail.

*sadighi@sharif.ir

II. MODEL

This simulation is based fundamentally on a model similar to the earlier papers [17,19–21]. An Ar bubble is described in SA aqueous solutions including the effects of water vapor diffusion, water vapor condensation and evaporation, conductive heat loss, and chemical reactions.

The bubble dynamics is described by the Rayleigh-Plesset equation, which takes sound loss and compressibility effects of the liquid into account and the van der Waals equation as the equation of state for gas inside the bubble,

$$\left(1 - \frac{\dot{R}}{C_l}\right) R \ddot{R} + \frac{3}{2} \left(1 - \frac{\dot{R}}{3C_l}\right) \dot{R}^2 = \left(1 + \frac{\dot{R}}{C_l}\right) \frac{1}{\rho_l} (P_g - P_a - P_0) + \frac{\dot{R}}{\rho_l C_l} \dot{P}_g - 4 \frac{\mu}{\rho_l} \frac{\dot{R}}{R} - \frac{2\sigma}{\rho_l R}, \quad (1)$$

$$P_g(t) = \frac{N_{\text{tot}}(t) k_B T}{V - N_{\text{tot}}(t) B}. \quad (2)$$

In these equations, R is the bubble radius, C_l is the velocity of the sound wave, ρ_l is the density of liquid, P_0 is the ambient pressure, P_a is the driving pressure, and P_g is the gas pressure. N_{tot} , μ , σ , and T are the total number of particles inside the bubble, the liquid viscosity, the liquid surface tension, and the gas temperature inside the bubble, respectively. The hard core parameter $B = 5.1 \times 10^{-29} \text{ m}^3$ is assumed to be equal for all particles.

The changes in particle number are modeled similar to the earlier processes, and they are explained very briefly [17,19–21]. Using the boundary layer formalism for mass diffusion, Ar and six chemically reactive species are considered. In this approach, eight chemical reactions are allowed [17,19–21]. The rate of a chemical reaction is calculated by the modified Arrhenius laws. The rate of change in the number of vapor molecules of particles inside the bubble is determined by their corresponding partial vapor pressure in the acid solution. The total rate of the change in species is given by equation,

$$\dot{N}_i^{\text{tot}} = \dot{N}_i^d + \dot{N}_i^c + \dot{N}_i^{\text{ec}}, \quad (3)$$

where \dot{N}_i^d is the rate of change in the particle number due to mass diffusion, \dot{N}_i^c is the rate of change in particle number i due to chemical reactions, and \dot{N}_i^{ec} is the rate of change in the number of vapor molecules due to evaporation and condensation.

Time evolution of the gas temperature is calculated from the energy equation of the bubble content,

$$\dot{T}_g \sum_j \frac{\partial e_{\text{th}j}}{\partial T_g} N_j = \dot{Q} - P_g \dot{V} \sum_j e_{\text{th}j} \dot{N}_j + \dot{E}_{\text{chem}} + \sum_j h_{w,j} \dot{N}_j^d, \quad (4a)$$

$$h_{w,j} = \left(1 + \frac{f_j}{2}\right) k_B T_0, \quad (4b)$$

$$e_{\text{th}j} = \frac{f_j}{2} k_B T_g + \sum_l \frac{k_B \Theta_{j,l}}{e^{\Theta_{j,l}/T_g} - 1}. \quad (4c)$$

The quantity \dot{E}_{chem} denotes the rate of change in the chemical energy of the bubble due to chemical reactions. Also, $e_{\text{th}j}$ is the thermal energy of the molecule with $\Theta_{j,l}$ as the various characteristic vibrational temperatures of the particle. The quantity $h_{w,j}$ is the molecular enthalpy of particle j at the bubble wall temperature T_g , and f_j is the sum of its translational and rotational degrees of freedom.

The boundary layer formalism used to consider the heat transfer \dot{Q} between the bubble and its surrounding liquid is given by

$$\dot{Q} = 4\pi R^2 \kappa \frac{T_0 - T_g}{l_{\text{th}}}, \quad l_{\text{th}} = \min \left(\sqrt{\frac{R\chi}{|\dot{R}|}}, \frac{R}{\pi} \right), \quad (4d)$$

where κ , l_{th} , and χ are the thermal conductivity coefficient of the gas inside the bubble, the thickness of the thermal boundary layer, and the thermal diffusivity coefficient of the bubble content, respectively.

Equations (1)–(4) are the set of coupled ordinary differential equations totally describing the evolution of the SL bubble that is solved numerically.

TABLE I. Physical parameters of various concentrations of SA solutions at different ambient temperatures.

SA	T (°C)	f_{res} (s ⁻¹)	C_l (m/s)	μ (gm ⁻¹ s ⁻¹)	σ ($\times 10^{-3}$ N/m)	ρ_l (Kg m ⁻³)	P_{water} (Pa)	P_{SA} (Pa)
0 wt %	0	34 059	1402.7	1.79	75.64	999.8	611	0
	10	35 147	1447.5	1.31	74.23	999.7	1230	0
	20	36 009	1483.0	1.00	70.70	998.0	2060	0
45 wt %	0	38 546	1587.5	7.14	70.60	1363.0	260	2.91×10^{-12}
	10	38 413	1582.0	5.73	70.40	1355.3	520	1.69×10^{-11}
	20	38 316	1578.0	4.60	70.10	1347.6	920	1.00×10^{-10}
50 wt %	0	38 486	1585.0	8.55	72.90	1411.0	193	1.09×10^{-11}
	10	38 364	1580.0	6.79	70.53	1402.9	405	7.69×10^{-11}
	20	38 243	1575.0	5.39	68.16	1395.1	802	4.74×10^{-10}
65 wt %	0	38 486	1585.0	15.04	63.50	1571.4	60	2.1×10^{-9}
	10	38 243	1575.0	13.02	63.20	1562.3	120	9.66×10^{-9}
	20	38 000	1565.0	11.05	62.90	1553.3	245	4.52×10^{-8}
85 wt %	0	37 636	1550.0	56.64	54.27	1800.9	0.343	1.21×10^{-5}
	10	37 199	1532.0	36.63	56.37	1789.7	0.952	4.9×10^{-5}
	20	36 956	1522.0	25.08	56.02	1778.6	2.45	1.79×10^{-4}

Physical parameters of various concentrations of SA at different temperatures, which are used in the simulation, are listed in Table I [22–24]. The ultrasound frequency used in the calculations was 38 kHz for 65 wt % SA at 20 °C, which changes with the temperature. All of the host liquids are saturated with 4 torr partial pressure Ar gas.

In order to have stable bubbles, three dominant instabilities named shape, diffusion, and position instability are considered. The procedure for considering these instabilities in the simulation was discussed before [17].

III. RESULTS

The stability conditions can be fulfilled simultaneously only in a certain region of (R_0, P_a) phase space. Considering the above mentioned instabilities, the phase diagrams in the (R_0, P_a) parameter space of various SA concentrations for different ambient temperatures are calculated. The resulting equilibrium curves for an Ar bubble at a partial pressure of 4 torr are shown in Figs. 1(a)–1(e) for 0 wt %, 45 wt %, 50 wt %, 65 wt %, and 85 wt % SA concentrations, respectively.

The shape instability is caused by the applied pressure changes in the spherical shape of the bubble wall, which results in a basic distortion of the SL bubble or even breaking it up. In Figs. 1(a)–1(e), the shape instability threshold is depicted where, at all points in the area below the threshold line, the perturbation of the bubble’s spherical shape is small, thus, the bubbles are stable. However, at all points in the regions above the threshold, bubbles will be unstable [2]. It should be realized that, in Figs. 1(d) and 1(e), some of these lines are not shown due to the larger R_0 where, in these regions, the shape stability is fulfilled.

Also in these figures, the curves of the threshold Bjerknes instabilities are shown. Bjerknes force is related to the acoustic pressure and is responsible for the bubble mean position [25].

The diffusion curves represent the points in the phase space with the zero net mass change in the bubble over one cycle. The gas contents of the bubble stay constant in time, which are not changed through diffusive mass exchange with dissolved gases in the liquid. The curves of the diffusion instability are represented in Figs. 1(a)–1(e). The points on the segments of the diffusion curve with the positive (negative) slope are stable (unstable). The points with the infinite slope are metastable [2,26]. The metastable points are called the threshold of the acoustic pressure at which the SL effect begins, depending on the host liquid temperature. The threshold pressure increases as the ambient temperature decreases, and the threshold radius almost is constant at about 2 μm .

The maximum stable bubble phase parameter is determined from the intersection of the diffusion curve with the dominant instability curve in each concentration and temperature. The highest light intensity corresponds to the largest achievable driving pressure on the diffusion curve. The obtained data from the numerical simulation for the Ar bubble, at the time of the maximum stable single bubble (the intersection points) for different concentrations of SA at different temperatures, are given in Table II.

In Fig. 1, the decrease in the ambient temperature leads to the shift in phase parameters of a stable SL bubble toward the higher pressure amplitudes in all concentrations of SA

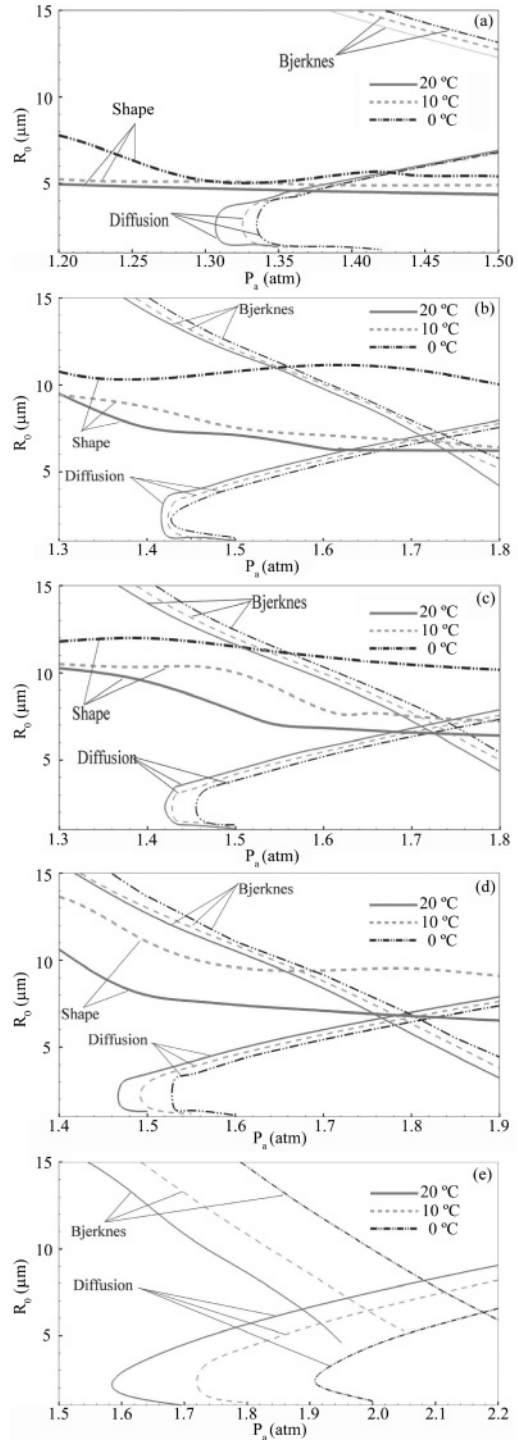


FIG. 1. Phase diagrams in the $R_0 - P_a$ space of the Ar bubble for different concentrations of SA at different ambient temperatures. (a) Water, (b) 45 wt % SA, (c) 50 wt % SA, (d) 65 wt % SA, and (e) 85 wt % SA.

solutions. In the intersection points, the higher the ambient temperature and the lower the SA concentration result in the more dominated shape instability. This trend, for the concentrated SA solutions in lower ambient temperatures, favors Bjerknes instability, which, in the boundary between the positional instability and the shape instability threshold MSBSL, is originated [3,8,9]. The shape instability depends

on the viscosity of the host liquid that strongly increases up to almost double (Table I), also, with decreasing its temperature, the viscosity, increased by the concentration of the SA, causes the bubble to be more stable. In other words, in SA solutions with higher viscosities, the bubble's surface perturbations damp out to become more stable in shape [10]. It should be realized that, based on the experimental measurements, the viscosity enhancement that produces larger bubbles is not the main reason for the increase in SL intensity. This was approved in the earlier experimental papers where they reported that they were not able to produce SBSL with SA, phosphoric acid, and glycerin at the higher concentrations [3,27]. Therefore, some other reasons, such as the vapor pressure, the bubble contents, and the amount of work performed on the bubble for the increase of intensity should be considered.

The time evolution of the radius of an oscillating bubble in one cycle is shown in Figs. 2(a)–2(e). The radius axis is normalized to R_0 in each temperature and SA concentration. In this figure, one can notice that, reducing the SA concentrations, the after bounces are increased due to the increase in the surface tension and the reduction in the density of the host liquid [2]. In SA, the time of the collapse is longer than that of water. For water, 45 wt % and 50 wt %, the order of collapse time first is 20 °C, which is followed by 10 °C and 0 °C; whereas, it is changed for 65 wt % and 85 wt %. According to these figures, the expansion ratios are almost 8 (Table II), which is about the same for all concentrations and temperatures. Since the bubbles consist of Ar noble gas, therefore, the expansion ratio is determined by the equation of mass diffusion applied to the Ar concentration relative to the saturation concentration according to previous papers [10].

Vapor pressure directly affects the number of particles penetrating the bubble. Partial vapor pressures of SA molecules and water molecules over different concentrations of SA solutions are given in Table I. It can be seen that the partial vapor pressures of water and SA decrease by a factor of 3 as the ambient temperature is reduced. Thus, it is expected that the number of existing water molecules in the bubble decreases. In Fig. 3, the number of water and Ar molecules

inside the SBSL bubble for different concentrations of SA at three different temperatures is indicated. For all mentioned SA concentrations, water vapor molecules decrease as the ambient temperature is reduced. The calculated amount of water vapor molecules directly determines the number of endothermic chemical reactions inside the bubble and the total chemical energy exchange as a part of the energy exchange given by Eq. (4a).

The terms of Eq. (4a) are calculated with a similar procedure as in our recent paper [17]. The calculation shows that there is a reduction in the chemical part of the energy exchanged with decreasing the ambient temperature due to the reduction in the number of water vapor molecules (see Fig. 3). The contribution of the chemical term is smaller than the first two terms in Eq. (4a). The main term in this equation is the work performed by the ultrasound field on the bubble.

The trend of change in the amount of the work performed on the bubble and the maximum SL intensity with the variation in ambient temperature are the same (see Fig. 4). In Fig. 4, the maximum SL intensity for different SA concentrations is indicated, which thermal bremsstrahlung mechanism of radiation is used to calculate the SL radiation similar to Yasui [13]. The variation in the ambient temperature changes the SL intensity. One can see that an increase in the ambient temperature for 0 wt % and 45 wt % SA concentrations causes the decrease in the maximum bubble temperature and the maximum light intensity. This is a similar behavior noticed experimentally in the water [10,13–16]. However, in the higher SA concentrations, 85 wt % and 65 wt %, in contrast to the lower concentrations, the increase in the liquid temperature increases the maximum bubble temperature and the maximum output power. At the SA concentrations around 50 wt %, it was very exciting to see that the radiation intensity is almost temperature independent. This was what was noticed in the experimental paper for a 65 wt % SA concentration [3], and it was an experimental paper limited down to 9 °C. However, these careful calculations clarify the point that the variations are small for the 65 wt % and 45 wt % where, for 50 wt %, it is almost constant. Furthermore, Fig. 4 indicates that, at

TABLE II. The bubble parameters presented at the time of maximum SL intensity for various concentrations of SA.

SA	T_0	P_a	R_0	T_{gmax}	R_{min}	R_{max}	Expansion ratio	$N_{Ar} (\times 10^{10})$
0 wt %	0	1.422	5.53	30 360	0.885	44.00	8.00	2.40
	10	1.388	4.92	29 190	0.772	39.75	8.08	1.65
	20	1.376	4.58	28 172	0.705	37.09	8.10	1.29
45 wt %	0	1.737	6.96	40 435	1.051	53.73	7.72	4.53
	10	1.701	6.80	40 759	1.013	52.70	7.75	4.08
	20	1.631	6.27	39 301	0.922	48.84	7.79	3.12
50 wt %	0	1.752	6.86	40 293	1.036	53.03	7.73	4.33
	10	1.730	6.90	41 182	1.028	53.13	7.70	4.25
	20	1.679	6.62	40 863	0.967	51.30	7.75	3.63
65 wt %	0	1.811	6.55	38 440	0.982	50.24	7.67	3.78
	10	1.789	6.63	39 835	0.981	50.85	7.67	3.74
	20	1.767	6.67	41 167	0.974	51.16	7.67	3.68
85 wt %	0	2.177	6.35	26 479	1.001	48.06	7.56	3.34
	10	1.991	6.43	33 010	0.967	48.76	7.58	3.37
	20	1.886	6.52	37 105	0.956	49.42	7.58	3.39

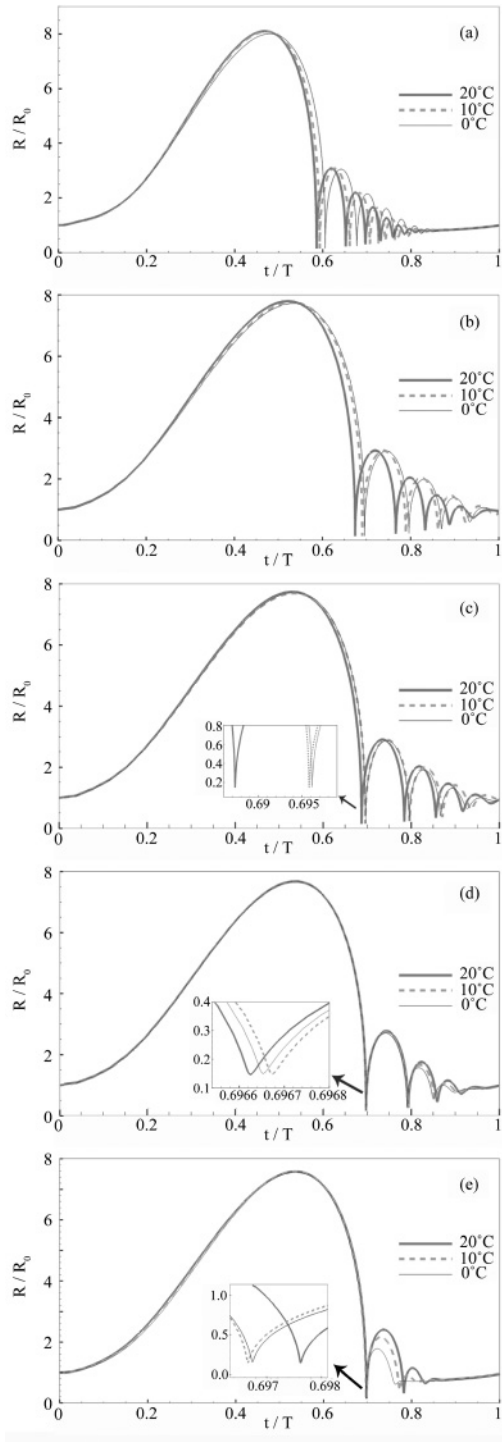


FIG. 2. Time evolution of the radius of bubbles during one period for different concentrations of SA. Equilibrium radii and ultrasound pressure are given in Table II. (a) Water, (b) 45 wt % SA, (c) 50 wt % SA, (d) 65 wt % SA, and (e) 85 wt % SA.

the higher concentrations of SA solutions, the light intensity is decreased, specifically for 85 wt % SA, and at the 0°C light intensity, it drops sharply and becomes less than that of water. This is in agreement with the experimental paper that the SL spectrum for bubbles of 4 torr Xe in the 85 wt % SA could not be observed where the total light emission for the water at 1°C and 85 wt % SA systems is almost

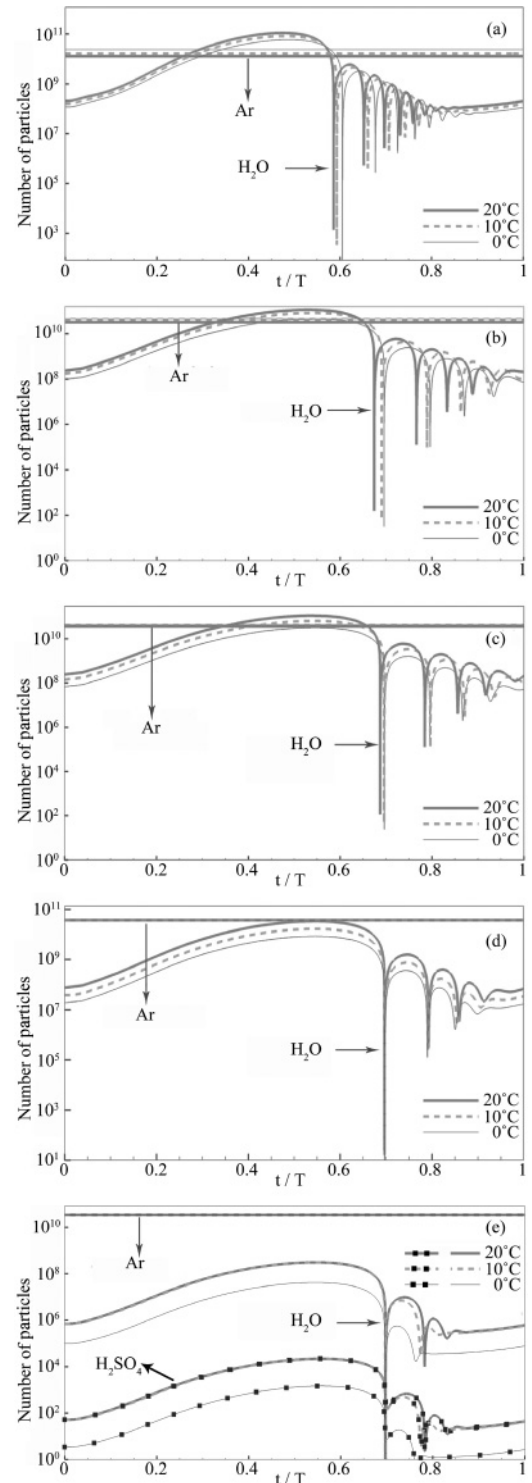


FIG. 3. The number of particles inside the SBSL bubble at the maximum achievable intensity for different concentrations of SA at different ambient temperatures. (a) Water, (b) 45 wt % SA, (c) 50 wt % SA, (d) 65 wt % SA, and (e) 85 wt % SA.

identical for xenon bubbles [4]. The maximum SL intensity for ambient temperatures of 20°C, 10°C, and 0°C occurred in SA solutions of 45 wt %, 50 wt %, and 65 wt %, respectively, and with decreasing the ambient temperature, the maximum

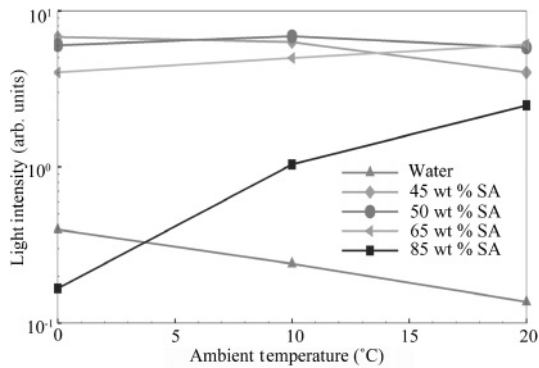


FIG. 4. The maximum SL intensity for different acid solutions versus ambient temperature. SL intensities have been normalized to the SL emission of 65 wt % SA at 20 °C.

bubble intensity shifts toward the lower concentrations of the SA solutions.

For more clarification about the results of SL, the ambient radius and the number of the Ar molecules inside the bubble are described. The increase in the ambient radius, which results in the increase in Ar inside the bubble, leads to the brightening of the SL. The ambient radius in aqueous SA is larger than the one in the water. Therefore, the number of Ar molecules in bubbles in SA is more than that of water. Hence, the SL in aqueous SA is brighter. On the other hand, it should be realized that, in the various SA concentrations, except 0 wt % (water), the ambient radii are almost identical, which leads one to conclude that the number of Ar molecules are roughly in the same order (see Table II). The intensity obtained from the bremsstrahlung mechanism directly depends on both the temperature and the number of Ar molecules inside the bubble. Thus, the intensity variation in different concentrations is mainly due to the variation in the maximum temperature inside the SL bubble. From Table II, it can be noticed that the maximum temperatures for three moderate concentrations of SA at different ambient temperatures are almost constant except for water and 85 wt % SA. The reduction in ambient temperature causes them to increase and to decrease, respectively.

The response of the Ar bubble in 85% SA to the ultrasound field is quite different from other SA concentrations based on two reasons. First, the main content (99% of the particles) of the bubble is Ar molecules, which decrease as temperature is reduced in contrast to the other concentrations. Since the Ar molecules are the source of bremsstrahlung radiation, there should be a decrease in SL radiation in 85% SA (see Fig. 4)

with a decreasing in the ambient temperature. In addition, the decrease in the amount of work performed on the bubble is another reason for the SL intensity reduction in 85% SA, which was explained before in detail.

The effect of other physical parameters, such as surface tension and liquid density is negligible due to their almost constant values in various temperatures. However, the increase in the surface tension reduces the peak temperature and the pressure during the collapse instant [28]. The surface tension of the various SA concentrations does not affect the temperature variations. An increase in liquid density yields slightly more violent implosions; however, the effect of this parameter is negligible because the density is almost constant as the ambient temperature is changed [28].

IV. CONCLUSIONS

The behavior of the Ar bubble in different concentrations of SA at different ambient temperatures was studied using the hydrochemical model. It can be concluded that some main parameters affected the SL intensity in various SA concentrations, such as vapor pressure, viscosity, and chemical composition, and the variation in these parameters with temperature and SA concentration affected the amount of work, maximum temperature, and SL light intensity of the bubble.

The maximum light intensity was calculated using a thermal-bremsstrahlung mechanism. Calculations indicated that, at the fixed degassing condition, each SA solution had a different response to temperature variations. The result was observed at a concentration of about 50 wt %, and it was the temperature independence of the output intensity for SL at this concentration. The calculations also indicated that, for a higher SA solution [85 wt %], the SL for a lower temperature dropped where it was less than that for water, and this was consistent with the experimental papers. Furthermore, it was found that, for 65 wt % SA, the maximum light emission occurred at the higher ambient temperatures. However, for lower 50 wt % and 45 wt % concentrations, the maximum intensity appeared at lower temperatures.

ACKNOWLEDGMENTS

The authors want to thank the research deputy of Sharif University of Technology for financial support of this project. The authors also want to thank Dr. Lotfi and A. Salehi for their useful comments.

-
- [1] D. F. Gaitan, L. A. Crum, C. C. Church, and R. A. Roy, *J. Acoust. Soc. Am.* **91**, 3166 (1992).
 - [2] M. P. Brenner, S. Hilgenfeldt, and D. Lohse, *Rev. Mod. Phys.* **74**, 425 (2002).
 - [3] A. Troia, D. M. Ripaa, and R. Spagnolo, *Ultrason. Sonochem.* **13**, 278 (2006).
 - [4] S. D. Hopkins, S. J. Putterman, B. A. Kappus, K. S. Suslick, and C. G. Camara, *Phys. Rev. Lett.* **95**, 254301 (2005).
 - [5] D. J. Flannigan and K. S. Suslick, *Phys. Rev. Lett.* **95**, 044301 (2005).
 - [6] D. J. Flannigan and K. S. Suslick, *Nature (London)* 434 (2005).
 - [7] R. Sadighi-Bonabi, N. Rezaee, H. Ebrahimi, and M. Mirheydari, *Phys. Rev. E* **82**, 016316 (2010).
 - [8] R. Sadighi-Bonabi, M. Mirheydari, N. Rezaee, and H. Ebrahimi, *Phys. Rev. E* **84**, 026301 (2011).

- [9] R. Sadighi-Bonabi, R. Rezaei-Nasirabad, and Z. Galavani, *J. Acoust. Soc. Am.* **126**, 62266 (2009).
- [10] G. E. Vazquez and S. J. Putterman, *Phys. Rev. Lett.* **85**, 3037 (2000).
- [11] M. Dan, J. D. N. Cheeke, and L. Kondic, *Phys. Rev. Lett.* **83**, 1870 (1999).
- [12] M. Dan, J. D. N. Cheeke, and L. Kondic, *Ultrasonics* **38**, 566 (2000).
- [13] K. Yasui, *Phys. Rev. E* **64**, 016310 (2001).
- [14] M. Germano, A. Alippi, A. Bettucci, F. Brizi, and D. Passeri, *Ultrasonics* **50**, 81 (2010).
- [15] R. Hiller, S. J. Putterman, and B. P. Barber, *Phys. Rev. Lett.* **69**, 1182 (1992).
- [16] S. Hilgenfeldt, D. Lohse, and W. C. Moss, *Phys. Rev. Lett.* **80**, 1332 (1998).
- [17] A. Moshaii, K. Imani, and M. Silatani, *Phys. Rev. E* **80**, 046325 (2009).
- [18] A. Moshaii, S. Tajik-Nezhad, and M. Faraji, *Phys. Rev. E* **84**, 046301 (2011).
- [19] X. Lu, A. Prosperetti, R. Toegel, and D. Lohse, *Phys. Rev. E* **67**, 056310 (2003).
- [20] R. Toegel and D. Lohse, *J. Chem. Phys.* **118**, 1863 (2003).
- [21] R. Toegel, S. Hilgenfeldt, and D. Lohse, *Phys. Rev. Lett.* **88**, 034301 (2002).
- [22] L. Gmelin and R. J. Meyer, *GmelinsHandbuch Der Anorganischen Chemie* (Verlag Chemie GmbH, Leipzig, 1985).
- [23] D. W. Green and R. H. Perry, *Perry's Chemical Engineers' Handbook*, 8th ed. (McGraw-Hill, New York, 2008).
- [24] D. D. Weerstra, U. S. Patent No. 5760297 (2 June 1998).
- [25] I. Akhatov, R. Mettin, C. D. Ohl, U. Parlitz, and W. Lauterborn, *Phys. Rev. E* **55**, 3747 (1997).
- [26] G. Simon, I. Csabai, Á. Horváth, and F. Szalai, *Phys. Rev. E* **63**, 026301 (2001).
- [27] D. F. Gaitan, A. A. Atchley, S. D. Lewia, J. T. Carlson, X. K. Maruyama, M. Moran, and D. Sweider, *Phys. Rev. E* **54**, 525 (1996).
- [28] D. Fuster, G. Hauke, and C. Dopazo, *Flow, Turbul. Combust.* **82**, 25 (2009).